water

MDPI

Article

Uranium and Nickel Partitioning in a Contaminated Riparian Wetland

Peng Lin [1,*], Maxim I. Boyanov [2,3], Edward J. O'Loughlin [2], Wei Xing [1], Kenneth M. Kemner [2], John Seaman [1,†], Steven P. Simner [4] and Daniel I. Kaplan [1]

[1] Savannah River Ecology Laboratory, University of Georgia, Aiken, SC 29803, USA; wei.xing@uga.edu (W.X.); seaman@srel.edu (J.S.); daniel.kaplan@uga.edu (D.I.K.)
[2] Biosciences Division, Argonne National Laboratory, Lemont, IL 60439, USA; mboyanov@anl.gov (M.I.B.); oloughlin@anl.gov (E.J.O.); kemner@anl.gov (K.M.K.)
[3] Institute of Chemical Engineering, Bulgarian Academy of Sciences, 1000 Sofia, Bulgaria
[4] Savannah River Mission Completion, Aiken, SC 29803, USA; steven.simner@srs.gov
* Correspondence: peng.lin@uga.edu
† Retired.

Abstract: Uranium (U) and nickel (Ni) released 50 years ago have been immobilized in the Tims Branch wetlands located on the Savannah River Site in the United States. Sediments were collected from seven locations to identify the factors responsible for this attenuation. Ni and U contents in the solids were significantly correlated, suggesting that depositional as opposed to chemical processes contributed to their spatial distribution. Based on sequential extractions, 63 ± 16% of the U was partitioned into the organic fraction, whereas Ni was distributed between several sediment fractions. An inverse pH-organic matter (OM) correlation and positive correlations of OM with total U and organic-bound U/Ni suggest that increased OM preservation and binding to the mineral surfaces were likely responsible for Ni- and especially U-sediment retention (Tims Branch pH = 4.84 ± 0.68). EXAFS analysis indicated the predominance of U(VI) coordinated with clay minerals (~65%), together with ~35% coordinated to either OM (in areas with elevated OM levels) or iron oxides. The desorption-K_d coefficients of U (3972 ± 1370 L/kg) and Ni (30 ± 8 L/kg) indicate that dissolved Ni poses a greater long-term risk than dissolved U for migrating downstream. This study suggests that a delicate balance of geochemical properties controls whether wetlands behave as sinks or sources of contaminants.

Keywords: radionuclides; monitored natural attenuation; organic matter; XANES; EXAFS; iron oxides; K_d

Citation: Lin, P.; Boyanov, M.I.; O'Loughlin, E.J.; Xing, W.; Kemner, K.M.; Seaman, J.; Simner, S.P.; Kaplan, D.I. Uranium and Nickel Partitioning in a Contaminated Riparian Wetland. *Water* **2024**, *16*, 966. https://doi.org/10.3390/w16070966

Academic Editors: Hrissi K. Karapanagioti and Vasileios Anagnostopoulos

Received: 1 March 2024
Revised: 20 March 2024
Accepted: 22 March 2024
Published: 27 March 2024

1. Introduction

Wetlands are highly reactive biogeochemical zones and critical ecosystems that serve to remove contaminants from surface waters and upwelling groundwater prior to reaching open waters [1–3]. The biogeochemistry of contaminants in wetlands is expected to be profoundly different than in uplands due to the unique hydrological regimes of wetlands. The prevalence of saturated soils often promotes the establishment of vegetation buffer zones, sediments with accumulated natural organic matter, elevated microbial activity, and sharp geochemical gradients (e.g., pH and dissolved oxygen) [4–6]. Together, these conditions can result in a diverse set of sediment properties and biogeochemical processes that can lead to the immobilization of organics, heavy metals, and radioactive elements [7–11], leading to wetlands being described as the "kidneys of the landscape" [12].

Between 1958 and 1989, the Tims Branch wetlands located on the Savannah River Site (SRS) in South Carolina received 43,500 kg of depleted uranium (U) as a result of accidental and purposeful discharges from several former U processing facilities [13–15]. Based on maps compiled from >700,000 gamma spectra and 8 sediment U depth profiles, it was

determined that 94% of the released U remained in the wetland [11], concentrated in five multi-hectare areas along the stream, accounting for ~11% of the land area adjacent to the stream. While land type (upland or wetland) and topography provided a reasonable first approximation of where much of the U was accumulated, hydrological watershed modeling revealed that the stream velocity was especially slow through many of the hot spots. Together with the fact that Tims Branch aqueous U concentrations are consistently below drinking water regulatory limits (30 μg/L, SRNS, 2015), this suggests that the system contains unique hydro-biogeochemical properties for sequestering the large mass of U in this contaminated area. Studies using field- and laboratory-controlled experiments have suggested different biogeochemical processes responsible for the strong U immobilization. For example, previous studies indicated that the availability of U, primarily present as hexavalent U(VI), was controlled by naturally occurring organic matter (OM) and amorphous iron oxides [13,16,17]. Furthermore, U binding can be promoted by rhizosphere OM, and co-association of U with root phosphate was also found [18–20]. However, the key geochemical processes controlling the immobilization of U in Tims Branch sediments are not sufficiently understood, particularly with respect to the array of U species and binding environments that may be present (e.g., U bound preferentially to OM or the iron oxides). Considering the increasing frequency and intensity of flooding events in recent years due to climate change, unidentified geochemical factor(s) in wetland sediments may be greatly altered, leading to an increasing concern that U mobility within the watershed may increase, leading to the contaminated area within Tims Branch eventually becoming a secondary source of U.

Nickel (Ni) and U, and lesser amounts of aluminum, chromium, mercury, and thorium, were discharged to Tims Branch. Wastes containing mixtures of radionuclides and heavy metals (as opposed to the release of a single contaminant) are common at Department of Energy sites and many other sites in the United States. Even when released together in the environment, the fate and transport of the individual contaminants (e.g., U and Ni) may vary if their chemical properties differ. A lower bioavailability of U compared to the co-contaminant Ni has been observed in Tims Branch wetlands [21,22]. Thus, the unidentified geochemical factor(s) in wetland environments, as aforementioned, can have a different impact on the immobilization/mobilization of U and Ni. It will be essential to understand the influence of such geochemical factor(s) on the biogeochemistry of heavy metals and its potential effect on radionuclide remediation strategies in co-contaminant scenarios.

Therefore, to fill the knowledge gap mentioned above, this study is designed and set up with a focus on exploring the unidentified geochemical factor(s) controlling the sorption/desorption of U and Ni, as well as investigating the U binding environments and speciation in Tims Branch wetland sediments. Seven wetland surface sediments were collected >5 m from the stream edge along Tims Branch. Besides total U and Ni measurements, sequential extractions were conducted to quantify the operationally defined solid-phase fractions that the U and Ni were associated with and to estimate the desorption distribution coefficients, K_d, which provide a measure of the tendency of U and Ni to desorb from the sediments. The results were correlated to several geochemical properties of the sediments (e.g., pH, OM, particle size distribution, X-ray diffraction (XRD)-mineralogy, and total Fe) to provide insight into the geochemical factor(s) that may be related to U and Ni binding to wetland sediments. Samples were also analyzed for U speciation by U L_{III}-edge X-ray absorption near-edge structure (XANES) spectroscopy to provide information about the U oxidation state and extended X-ray absorption fine structure (EXAFS) spectroscopy to determine the U binding environment.

2. Materials and Methods

2.1. Sampling

Six contaminated surface sediment samples were collected in November 2019 (~30 years after the cessation of waste discharge) from the Tims Branch wetlands, including three samples (#2303, #2304, and #2305) from the Beaver Pond location and three samples (#2300,

#2301, and #2302) from the Steed Pond location (Figure 1). A control sediment sample was collected from an upstream area (#2306, Figure 1). It should be noted that, in contrast to commonly saturated wetland sediments, the collected sediments were rarely saturated after the beaver dam (Beaver Pond) and the man-made dam (Steed Pond) were breached in the late 1980s, exposing the pond floor to the atmosphere.

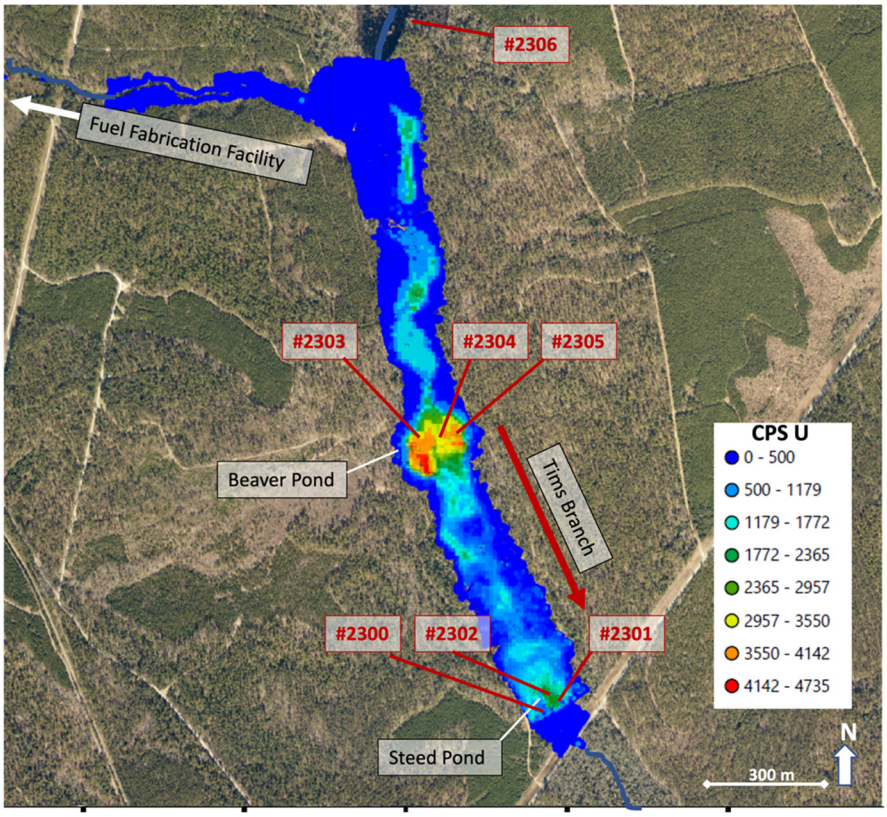

Figure 1. Sampling locations identified on a heat map of U concentrations (counts per second, CPS; map based on data from Kaplan et al. [23]) of the Times Branch wetland, Savannah River Site (SRS). The U and Ni sources (Fuel Fabrication Facility), the upstream sediment sample (#2306), and the contaminated sediment samples (#2300–#2305) are noted. The heat map shows the spatial distribution of U activity in Tims Branch, especially showing the high concentration of U in Beaver Pond (1772 to 4735 CPS U) and Steed Pond (1772 to 2957 CPS U). The U activity on the heat map was determined from the gamma radiation produced by ^{234m}Pa (a daughter product of ^{238}U, corrected for background) in >700,000 gamma spectra.

Samples were collected by first removing the leaf litter and then recovering about one kg of sediment (to a depth of 10 cm) using a hand spade. At the time of sampling, the water table was between 0.4 and 0.9 m below the ground surface, so the sediment samples were not saturated with water. Samples were stored in their field-moist state in zip-lock bags at 5 °C without taking precautions to eliminate air.

2.2. Sediment Characterization

All experiments were conducted with sediments that were air dried for one week and then passed through a 2-mm sieve. Select measurements were also made on the dried clay-size fraction (<2 μm) of these sediments that were collected by standard methods involving gravitational settling of a sediment suspension following the principles of Stokes Law [24]. Standard methods were used for general sediment characterization in duplicate or triplicate samples [25]. pH was determined from a 1:1 sediment:water suspension. Particle size distribution was determined using sieves for the sand fraction (2 μm–0.05 mm), a hydrometer for the clay size fraction (<2 μm), and by calculating the sand-clay differential

to determine the silt size fraction (i.e., silt = total − sand − clay). For the determination of OM in sediments, two methods were applied in this study. The loss-on-ignition (LOI) method was used to determine the bulk OM concentrations. Briefly, the samples were initially dried at 105 °C, followed by ignition in a muffle furnace for 2 h at 360 °C. The weight loss after the ignition was obtained to represent the OM concentrations. On the other hand, total carbon and nitrogen in sediments were determined by combustion/IR detection (LECO CNS-2000 analyzer, St. Joseph, MO, USA). Because these are acidic sediments, they contain negligible amounts of inorganic carbon. As such, the measurements can be considered measures of total organic carbon (TOC) and total nitrogen (TN). Total free Fe was measured by the dithionite-citrate-bicarbonate extraction method, which provides a measure of the amorphous and crystalline iron oxides but not the iron within clay mineral phases D [25]. This measurement was selected to represent the iron fraction that is most geochemically active. Total sedimentary U and Ni concentrations were determined by digesting 0.25 g of homogenized samples using concentrated HNO_3 (heated to 95 °C) and 30% H_2O_2 per the EPA 3050B method [26]. It should be noted that it does not digest some of the most recalcitrant fractions, such as silicates and refractive oxides, and, as such, may slightly underestimate the actual total U and Ni concentrations. An aliquot of each digestate was analyzed in a 2% HNO_3 matrix via ICP-MS (Thermo X-Series II). In addition to a water blank, a NIST sediment standard #8704 was carried through the digestion and ICP-MS analyses. All digestions and analytical analyses were conducted in duplicate. Randomly oriented powder mounts of the <2 μm sediment fraction were prepared for XRD (Bruker D2 PHASER) analysis using standard methods [27]. For XRD analysis, 1 g of each sediment sample was ground in isopropanol using a McCrone Micronizing Mill to obtain a fine powder. XRD patterns of the samples were collected from 3° to 75° 2θ with a 0.02° 2θ step-size, integration time of 0.5 s per step, and 30 rpm for the sample rotation speed. Phase identification was conducted using the Bruker DIFFRAC.EVA software (V7) by comparing each XRD trace to reference patterns in the PDF-4+ database (2023) compiled by the International Center for Diffraction Data (ICDD). Phase proportions were determined via Rietveld analysis using Bruker DIFFRAC.TOPAS. Samples were mixed with National Institute of Standards and Technology (NIST) Silicon Standard Reference Material (SRM) 640f to enable the determination of amorphous phase proportions.

2.3. Sequential Extraction of Sediments

Sequential extractions of U and Ni were conducted on each sediment, according to the methods described in [28]. Additional details about the procedure are presented in Supporting Information and Table S1. Briefly, the method included the following four sequential extractions: (1) saturated paste extract ($C_{SatPaste}$; 1.0:0.4 DI-water:sediment), (2) exchangeable extract (C_{Exch}; overnight extraction with 25:1 liquid:solid; acetic acid; 0.44 M CH_3COOH + 0.1 M $Ca(NO_3)_2$), (3) organically bound extract (C_{Org}; 25:1 liquid:solid; sodium pyrophosphate: 0.1 M $Na_4P_2O_7$ extraction), and (4) amorphous Fe-oxide extract (C_{AmFeOx}; 25:1 liquid:solid; acidified ammonium oxalate: pH 3 (0.175 M $(NH_4)_2C_2O_4$ + 0.1 M $H_2C_2O_4$). Additionally, the total U and Ni concentrations estimated from the acid digestion of the whole sediment in Section 2.2 were used to estimate the residual fraction ($C_{residual}$), calculated by subtracting the U and Ni mass in the four sequential extractions from the mass in the total U and Ni. Regarding the organic fraction defined as the pyrophosphate extractable fraction, Kaplan and Serkiz [28] demonstrated that this extractant is effective at extracting OM bound to sediment surfaces and does not complex U, presumably due to its polyphosphate molecular structure. Together, these data were also used to calculate $K_{d-desorb}$ values (L/kg):

$$K_{d-desorb} = \frac{C_{solid}}{C_{aq}} = \frac{C_{Exch} + C_{Org} + C_{AmFeOx}}{C_{SatPaste}} \quad (1)$$

where C_{Exch}, C_{Org}, and C_{AmFeOx} are the Ni or U concentrations in the solid phase, C_{solid}, extracted by the dilute-acid extract, organically bound extract, and amorphous Fe-oxide

extract (mg/kg), respectively. $C_{SatPaste}$ is the Ni or U concentration in the aqueous phase extracted from the saturated paste extract (mg/L). The three extracts used to define C_{solid} are intended to represent the Ni or U bound phase(s) that may eventually enter the mobile aqueous phase under a wide range of environmentally relevant conditions. As such, they are not intended to represent the fraction of Ni and U occluded in silicates, aluminosilicates, crystalline Fe-oxides, and crystalline Mn-oxides or present in sparingly soluble precipitated phases (i.e., the residual fraction in the sequential extraction sequence described previously). Important advantages of this approach to measuring K_d values as opposed to the batch-adsorption method, in which solute is added to an uncontaminated sediment, are that the $K_{d-desorb}$ does not require that the researcher guess the solute speciation or concentration, and it has the benefit of using sediment with the contaminant aged under field conditions.

2.4. Uranium X-ray Absorption Spectroscopy

X-ray absorption near edge structure (XANES) and extended X-ray absorption fine structure (EXAFS) spectra were collected from the dry whole sediment and the <2 μm fractions at the U L_{III}-edge (17,166 eV) in fluorescence mode using a 4-element Si drift detector (Vortex-ME4, Hitachi). The samples were packed into 3 mm thick, drilled plastic slides and sealed with Kapton film. Samples were transported to the MRCAT/EnviroCAT Insertion Device beamline (Sector 10, Advanced Photon Source) [29] and measured in the ambient atmosphere at room temperature. Radiation-induced changes in the spectra were not detected during measurements made at six discrete locations on the sample. XANES and EXAFS data from U minerals, U complexed in solution, and standards of U(VI) adsorbed to various surfaces, such as carboxyl-functionalized beads, iron oxides, and clays, were measured during this and previous studies at the same beamline [30–33]. Energy calibration was established by setting the inflection point in the spectrum of a hydrogen uranyl phosphate standard to 17,166 eV and maintaining it through frequent or concurrent collection of data from the standard.

Normalization and background removal of the data were conducted using the AUTOBK program [34]. Linear combination fits of the data were performed using the ATHENA program [35].

3. Results and Discussion

3.1. Sediment Properties

Tims Branch sediments were acidic, ranging from pH 4.25 to 6.13 with an average pH of 4.84 ± 0.68 (Table 1 and additional details presented in Table S2). Sediment particle size distributions varied greatly, ranging from silty clay to sand-textured sediments. As expected, the OM concentrations were relatively high, ranging from 4 wt-% to 30 wt-% of the total mass (Table 1). Within the OM pool, the TOC concentrations varied from 22.5 g/kg to 119.9 g/kg, while TN ranged from 1.2 g/kg to 8.3 g/kg (Table 1). As noted previously, sediment free-Fe concentration measurements provide a measure of the Fe on mineral surfaces, including Fe-oxide coatings; the concentrations measured for this study were consistent with previously reported values [28], with the exception of the unusually low value for sediment #2301 of 0.24 wt-%. The clay fraction of the seven sediments had similar mineralogy, as identified by XRD (Table S3). The amorphous materials (presumably, non-crystalline silicates, iron-, aluminum-, and manganese-oxides) and kaolinite accounted for over 60 wt-% of the solids in the samples, while quartz accounted for between 6.8 and 29.1 wt-%, and gibbsite, goethite, and hematite, together, accounted for <10 wt-% of the clay-size fraction. More detailed information regarding pattern analysis, goodness of fit, and semi-quantitative mineralogy results is presented in Supplemental Information and Table S3. This mineralogy is consistent with previous measurements of local sediments [36], with the exception of Kaplan [37], which occasionally detected 2:1 clays that were identified as hydroxy-interlayered vermiculite.

Table 1. Sediment characterization, including pH, organic matter abundance (OM), total organic C (TOC), total N (TN), free Fe concentrations, and the clay/silt/sand distribution.

	Upstream Sample (#2306)	Contaminated (#2300–#2305)			
		Average	Std. Dev.	Min.	Max.
pH	6.13	4.63	0.41	4.25	5.37
OM (LOI), wt-%	8	22	10	4	30
TOC, g/kg	22.5	72.9	34.7	28.4	119.9
TN, g/kg	1.2	5.4	2.3	1.9	8.3
Clay, wt-%	22	35	16	6	51
Silt, wt-%	37	10	4	5	17
Sand, wt-%	42	55	18	41	89
Free Fe, wt-% [a]	1.42	2.15	1.20	0.24	3.45

Note: [a] Free Fe is a measure of the amorphous and crystalline iron oxides and does not include Fe associated with the clay mineral structure.

With respect to correlating sediment properties, there was a significant positive correlation between OM and free Fe (r = 0.925, $p \leq 0.01$, Figure S1) and between OM and clay (r = 0.811; $p \leq 0.05$, Figure S1) (Table 2), suggesting the preferential sorption or association of OM to these sediment components with large specific surface areas, relative to OM association with the sandy and silt particles [38,39]. pH was inversely and highly correlated with OM concentrations (r = 0.906, $p \leq 0.01$, Table 2). This trend has been attributed to: (1) OM taking on a more globular structure (more surface adhering structure), as opposed to a less coiled, more linear structure, at lower pH levels, and (2) the pH-dependent charges of OM taking on a more positive charge at lower pH values, thereby promoting greater electrostatic attraction to permanent-charge mineral surfaces with more negative charges [40]. Also, acidic conditions promote OM to take on more condensed supramolecular structures that can promote greater hydrophobic attraction to surfaces, as compared to under more basic conditions, which can promote repulsion of negatively charged ligands and expansion of its supramolecular structure [41]. Furthermore, lower pH environments can delay OM mineralization and lead to the stabilization of OM by retarding the activities of microorganisms [42,43]. Therefore, it can be expected that the acidic conditions at Tims Branch would facilitate the stabilization and preservation of OM in these sediments.

Table 2. Pearson correlation coefficients, r, for sediment properties measured in Tims Branch sediments.

	Clay (wt-%)	pH	OM (wt-%)	Free Fe (wt-%)	Ni (mg/kg)
pH	−0.674				
OM (wt-%)	**0.811** *	**−0.906** **			
Free Fe (wt-%)	0.724	−0.730	**0.925** **		
Ni (mg/kg)	0.476	−0.435	0.387	0.071	
U (mg/kg)	0.664	**−0.790** *	**0.786** *	0.529	**0.846** **

Notes: * Significant correlation at $p \leq 0.05$ (critical r value ≥ 0.754). ** Significant correlation at $p \leq 0.01$ (critical r value ≥ 0.833).

As is common in many contaminated sediments, the levels of contamination at Tims Branch varied greatly: 52 to 3806 mg/kg Ni and 71 to 7479 mg/kg U (Table 3). The samples were collected along two transects. The Beaver Pond transect (samples #2303, #2304, and #2305) was about 2 km from the source term, and the Steed Pond transect (samples #2300, #2301, and #2302) was a hot spot located about 4 km downstream. There were no significant differences in Ni/U averaged concentrations between the two locations according to the *t*-test ($p < 0.05$) (e.g., 4256 ± 3797 mg-U/kg at Steed Pond vs. 4875 ± 912 mg-U/kg at Beaver Pond, Table S4), and, for that reason, their concentrations were pooled together and reported in Table 3 as a single mean for all 6 contaminant locations. The concentration of Ni in the downstream contaminated areas was as much as 60 times greater than in the samples from the upstream area (e.g., #2300 vs. #2306), with an average concentration of

1774 ± 1448 mg/kg in contaminated areas (Table 3). A similar situation was found for the total U concentration, ranging from 22 mg/kg in #2306 sediment to as high as 7479 mg/kg in contaminated sediment (Table 3). Total Ni and U concentrations were highly correlated to each other (r = 0.846; $p \leq 0.01$, Table 2). Because the biogeochemistry of these two elements is significantly different, this observation suggests that depositional processes may have had a greater impact on contaminant distribution in the wetland than subsequent biogeochemical processes. Unexpectedly, the sediment sample collected upstream of the Fuel Fabrication Facility tributary #2306 (Figure 1) had greater concentrations of U (22 mg/kg U) and Ni (72 mg/kg Ni) than the reported site-specific background levels of approximately 1 mg U/kg [30] and 2.2 mg Ni/kg [44]. It is possible that the upstream sediments were affected by the fact that the upstream location was at some previous time under flooded conditions, permitting greater water transmissivity upgradient than presently exists.

Table 3. Ni and U total sediment concentrations, desorption coefficients ($K_{d-desorb}$; Equation (1)), and clay-fraction enrichment factors.

	Upstream (#2306)	Contaminated (#2300–#2305)			
		Average	Std. Dev.	Min.	Max.
Nickel					
Total Ni, mg-Ni/kg	72	1774	1448	52	3806
Clay Ni, mg-Ni/kg-clay	213	1729	1088	543	3132
Clay-fraction enrichment [a]	3.0	2.6	3.9	0.8	10.4
$K_{d-desorb}$, L/kg	185 ± 17	30	8	16	36
Uranium					
Total U, mg-U/kg	22	4566	2474	71	7479
Clay U, mg-U/kg-clay	57	3744	1626	517	4952
Clay-fraction enrichment [a]	2.6	1.9	2.6	0.7	7.3
$K_{d-desorb}$, L/kg	737 ± 203	3972	1370	2812	6275

Note: [a] Clay-fraction enrichment = $C_{clay\text{-}U/Ni}/C_{total}$, where $C_{clay\text{-}U/Ni}$ is the concentration of U or Ni in the clay fraction of sediments (mg/kg-clay) and $C_{clay\text{-}U/Ni}$ is the total U or Ni concentration in the sediments (mg/kg).

3.2. Partitioning of Ni and U in Sediments

3.2.1. Clay-Fraction Enrichment of Ni and U

Ni and U concentrations in the clay fractions (<2 μm) were compared to those in the whole sediments (Table 3). Metal contaminants are expected to be enriched in the clay-sized particles due to their greater specific surface areas (m^2/g) and greater abundance of OM and iron hydroxide coatings. However, the clay-fraction enrichment was only observed in the significantly less contaminated #2306 and #2301 sediments (Table S4). Ni accumulated in the clay fraction with enrichment factors of 3.0 and 10.4 in #2306 and #2301, respectively, while U clay-fraction enrichment was 2.6- and 7.3-fold, respectively (Table S4). Kaplan and Serkiz [28] reported that the clay-size fraction did not enrich U or Th at another contaminated wetland site on the SRS, similar to our observations in most of the downstream sediments (e.g., clay-fraction enrichment of U: 0.7 in #2300, 0.8 in #2302, 0.9 in #2303, 0.8 in #2304, and 0.9 in #2305, Table S4). Based on scanning electron microscope (SEM) images of SRS sediments, a previous study [45] found the silt (2 to 50 μm) and sand (50 to 2000 μm) grains possessing iron oxides and natural OM coatings that can be especially effective at binding metals, thereby increasing the effective particle surface area and reducing the tendency for clay-fraction enrichment of sorbed U or Ni observed in most of our downstream contaminated sediments.

3.2.2. Solid-Phase Distribution of Ni and U

Past studies have attempted to identify the components of a sediment responsible for binding contaminants using selective extraction techniques [46–48]. Importantly, these selective or sequential extraction techniques have experimental limitations that include the

non-selectivity of extraction reagents for given sediment phases or the re-adsorption of extracted contaminants onto other surfaces. Thus, sediment components targeted by the specific sequential extraction procedure may not adequately represent the discrete sediment phase(s) to which the contaminant is bound, that is, the distribution of the contaminant among sediment compartments is operationally defined by the extraction process.

As shown in Figure 2 and Table S5, over 30% of the total Ni concentration was evenly distributed in the exchangeable and the amorphous Fe-oxide-associated fractions of the upstream sediment (i.e., #2306), leaving 26% of total Ni in the organic fraction and only 4% for the structural fraction. The sediments collected from the contaminated portion of Tims Branch tended to have significantly more structural Ni. On average, in the contaminated areas, the Ni distribution between fractions followed the general order: structural fraction (33 ± 22%) > exchangeable (27 ± 8%) ≈ amorphous Fe oxide (27 ± 8%) > organic fraction (14 ± 8%). Compared with the upstream sample, this suggests that a greater percentage of the Ni in the contaminated regions was associated with more geochemically refractory fractions (e.g., precipitated Ni and fractions associated with crystalline Fe-oxide or Mn-oxides).

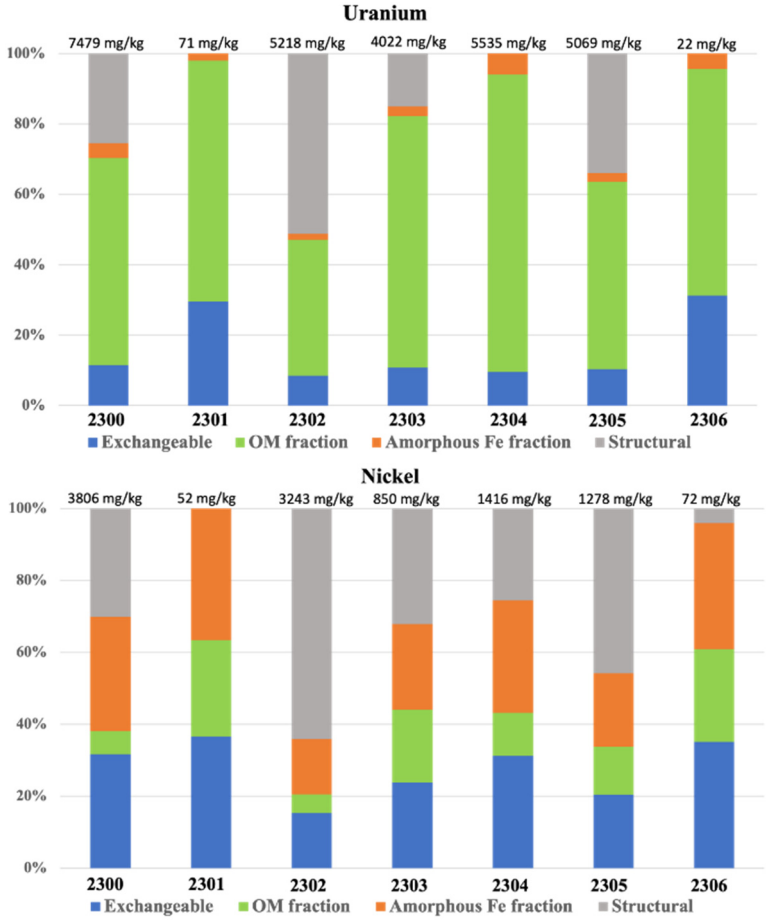

Figure 2. Solid-phase distribution of U and Ni among fractions in Tims Branch sediments. The values on the top of the bars show the total concentrations of U and Ni in each sediment. Samples #2300–#2305 were collected from the contaminated area, and #2306 was collected from an upstream area.

In contrast to the solid-phase distribution of Ni, 63 ± 16% of the U was associated with the organic fraction (Figure 2 and Table S5). Relatively lower but significant concentrations of U were present in the exchangeable fraction at the upstream site (31% at #2306) but decreased to 13 ± 8% in the six downstream sediments (i.e., #2300–#2305). A low abundance of U in the amorphous Fe oxide-associated fraction was observed in all sediments (<5%),

with no significant difference between contaminated and upstream areas (Figure 2). Similar to Ni, a considerable fraction of U in the contaminated sediments was present in the residual "structural" pool, especially for #2302 and #2305 sediments, where >30% of the total U was associated with crystalline Fe oxide or other solid phases containing U.

3.2.3. Desorption Distribution Coefficients ($K_{d-desorb}$)

To evaluate the potential mobility of U and Ni, $K_{d-desorb}$ values were derived from the sequential extraction data (Equation (1), Section 2.3). The estimated U and Ni $K_{d-desorb}$ values are summarized in Table 3 (and Figure S3, Table S4). Consistent with the higher percentage of saturated paste extracted Ni in comparison to U (i.e., the fraction that is most readily released, <0.02% for aqueous U vs. ~0.5% on average for aqueous Ni), the $K_{d-desorb}$ values for U were generally two magnitude orders higher than those for Ni (3972 ± 1370 L/kg for U vs. 30 ± 8 L/kg for Ni), with a range from 2812 L/kg to 6275 L/kg for U and 16 L/kg to 36 L/kg for Ni, respectively (Table 3). The correlation of U $K_{d-desorb}$ with different sediment characteristics was generally quite weak (Table 4), even with those sediment parameters for which strong correlations were found with the total U or the various sequentially extracted U fractions (e.g., for pH-total U, r = 0.790 ($p \leq 0.05$); for OM-total U, r = 0.790 ($p \leq 0.05$); for total N-Organic U, r = 0.773 ($p \leq 0.05$); Table 4). One possible explanation for these weaker U $K_{d-desorb}$ correlations may be that U partitioning to the solid phase was affected by a combination of geochemical factors, for example, the potential influence of coupling of pH and OM on metal partitioning to sediments (discussed in Section 3.3). It should be mentioned that the correlations of Ni $K_{d-desorb}$ with different sediment properties are not presented here since Ni $K_{d-desorb}$ values in most of the contaminated sediments fell in a narrow range between 32 and 36, except for the upstream sample, #2301 (Table 3).

Table 4. Pearson correlation coefficients (r) for the correlation between sediment properties and different solid phases of Ni and U in Tims Branch sediments.

	Nickel				**Uranium**			
	Ni_{acid} (mg/kg)	**Ni_{org} (mg/kg)**	**Ni_{AmFeOx} (mg/kg)**	**Ni $K_{d-desorb}$ (L/kg)**	**U_{acid} (mg/kg)**	**U_{org} (mg/kg)**	**U_{AmFeOx} (mg/kg)**	**U $K_{d-desorb}$ (L/kg)**
pH	−0.453	**−0.822** *	−0.399	-	**−0.757** *	**−0.809** *	−0.628	0.413
OM (wt-%)	0.399	**0.834** **	0.368	-	0.748	**0.831** *	0.643	0.186
Free Fe (mg/kg)	0.109	0.603	0.079	-	0.503	0.628	0.426	0.082
TOC (mg/kg)	0.242	0.658	0.162	-	0.581	0.626	0.402	0.218
Total N (mg/kg)	0.514	**0.829** *	0.450	-	**0.780** *	**0.773** *	0.585	0.220

Notes: * Significant correlation at $p \leq 0.05$ (critical value ≥ 0.754). ** Significant correlation at $p \leq 0.01$ (critical r value ≥ 0.833). "-" Correlations of Ni $K_{d-desorb}$ with different sediment properties were not present because of the narrow range of Ni $K_{d-desorb}$ values.

A comparison of the $K_{d-desorb}$ of Ni and U (Table 3) clearly suggests that Ni would tend to desorb from contaminated sediments and enter the mobile aqueous phase more readily than U. This is also consistent with the greater fraction of exchangeable Ni in all sediment samples than the fraction of exchangeable U (Figure 2). In addition, our estimated Ni $K_{d-desorb}$ values on average (Table 3) appeared to fall within the range of Ni $K_{d-desorb}$ values reported in other environments (e.g., 2.52 L/kg in Shadegan Wetland, Iran [49]; 5.2 L/kg in Hoor Al-Azim wetland, Iran [50]; 190 L/kg in the clay layer of Lastensuo Bog, Finland [51]; and 1500 L/kg at Tajikistan [52]). It has been demonstrated that the desorption of Ni in the sediment will increase at low pH, especially for the fulvic/humic acid-enriched sediments where Ni is complexed by these relatively more mobile organic ligands [51]. For example, the $K_{d-desorb}$ value for Ni (Table 3) in high-pH sediment from the upstream area (pH = 6.13, #2306, Table 1) was about 5 times higher than that for the two pond sediments

with a lower pH (pH = 4.63 ± 0.42, Table 1). Similarly, compared with the high Ni K_d values reported at Tajikistan sediments with a pH > 7.5 (1500 L/kg [52]), our lower Ni $K_{d-desorb}$ values may also be related to the acid nature of Tims Branch sediments (Table 1).

For U, the estimated $K_{d-desorb}$ values in the contaminated Tims Branch sediments were of the same magnitude as those of previously measured values at other wetlands on the SRS [28]. Our observed U $K_{d-desorb}$ values (Table 3) were typically higher than those measured in several different environments (e.g., 71 L/kg to 390 L/kg at Karnataka, India, [53]; 91 at Tajikistan, [52]; and 276–2249 L/kg at forest sites at Los Alamos National Laboratory, [54]). Therefore, in contrast to some environments where U is quite mobile, such as carbonate systems, the relatively large $K_{d-desorb}$ values measured in this study suggest that the U in Tims Branch watersheds will largely remain attached to the sediments, providing quantitative data for understanding why 94% of the inventory of U remains in this wetland study site 50 years after U release into the nearby stream [11].

3.3. Coupling Effects of pH and Organic Matter on Ni and U Immobilization

Total U concentrations were significantly and positively correlated with OM concentrations (r = 0.786, $p \leq 0.05$, Table 2), corresponding with the large organic-bound U fraction (U_{org}) (Figure 2) and the significant correlation between U_{org} and OM (r = 0.831, $p \leq 0.05$, Table 4). Significant OM correlations also existed for the operationally defined organic-bound Ni (r = 0.834, $p \leq 0.01$, Table 4), while no correlation was observed between the total Ni and OM due to the low contribution of the Ni_{org} fraction to the total Ni pool. Given the significant negative correlation between pH and OM (r = −0.906, $p \leq 0.01$, Table 2), the negative correlation of pH with total U (r = −0.790, $p \leq 0.05$, Table 2), the negative correlation of pH with organically bound U, and the negative correlation of pH with organically bound Ni can be expected (r = −0.809 for U_{org} and r = −0.822 for Ni_{org}, $p \leq 0.05$; Table 4 and Figure S2).

Combining the correlations of U/Ni with the pH and OM mentioned above, the pH-OM coupling effect can be proposed as the key driver for the accumulation and transport of the two contaminants. Such pH-OM coupling effects are consistent with several previous studies that used natural OM in laboratory batch experiments, showing the enhancement of U sorption by OM under low pH conditions [55,56]. The batch experiments by Velasco et al. [57] also suggested that the pH-OM coupling effect on the increased U precipitation/sorption can be relevant to radioactive waste repositories, wetlands, and other organic-rich environmental systems. Therefore, these field observations also support that a pH-OM coupling effect exists for metal binding in sediments. The acidic nature of the organic-rich Tims Branch wetland sediments would further enhance OM preservation, consequently promoting the immobilization of contaminants, like U, that have a strong association with OM. For example, high accumulation of U occurred in Beaver Pond sediments with a pH of 4.32 ± 0.07 and a high OM content (29 ± 1%) (Table 1). It is noteworthy that within the OM pool, TN contents in the collected sediments were strongly related to both U and Ni bound with organic fractions (Table 4 and Figure S2), while TOC concentrations showed no correlation with the different solid phases of U and Ni. One explanation for these combined correlations is that organic U and Ni in Tims Branch sediments are mostly associated with N-containing organic compounds. For U, our observed correlation supports previous Fourier-transform Ion Cyclotron Resonance Mass Spectrometry (FTICR-MS) measurements showing that Tims Branch rhizosphere sediments containing more N-containing functional groups and more heteroatoms (i.e., nitrogen, sulfur, and phosphorus) have much greater U concentrations than non-rhizosphere sediments [36]. Thus, our observation provides further support for the supposition that N-containing organic compounds have an important role in binding U. Nevertheless, such indirect evidence does not indicate that either U or Ni directly bonded to or were complexed with N-containing organic compounds. Other minerals that adsorbed or occluded with sedimentary OM in low pH conditions can still potentially provide the direct binding

ligands for the U or Ni, which required further investigation by spectroscopic techniques (see discussion below).

3.4. U Speciation in the Sediment

The U L_{III}-edge XANES data from five clay fractions (#2300–#2304) and two whole sediments (#2300 and 2302) are compared to U(VI) and U(IV) standards in Figure 3A. All spectra overlay each other and the U(VI) standard, indicating the predominance of U(VI) at the sampled locations. Linear combination fits of the XANES data quantify the U(VI) content in the range of 96–100% (Figure S4). The remaining U(IV) fraction resulting from the analysis is within the ±5% uncertainty, so the presence of reduced U species cannot be ascertained.

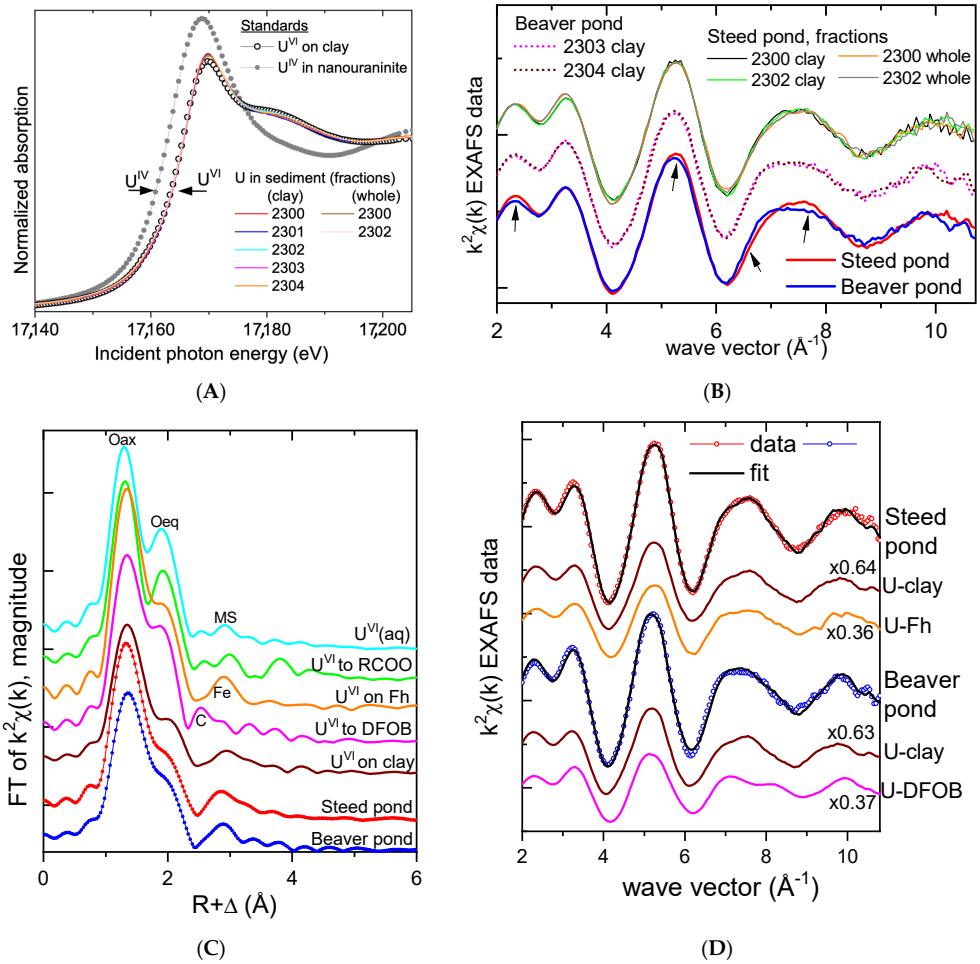

Figure 3. (**A**) U L_{III}-edge XANES spectra from the sediments collected at the indicated locations, compared to U(VI) and U(IV) standards. (**B**) $k^2\chi(k)$ EXAFS data; top spectra are from the whole sediments collected at two Steed Pond locations and from their clay fractions; middle spectra are from the clay fractions obtained from two Beaver Pond locations; the red and blue line spectra at the bottom show the average of the top and middle spectra, respectively. The arrows highlight the spectral differences at the two locations. (**C**) Fourier transforms of the averaged data from the two sampling areas (symbols) compared to relevant standards from prior studies (see text). Some spectral features assigned to atomic shells during the analysis of these standards are noted. Oax and Oeq are axial and equatorial O; MS = multiple-scattering from Oax, which also contributes partially to the adsorbed U spectra around 2.8 Å; (**D**) best fits from the linear combination analysis of the EXAFS data; the fit components and scaling factors are shown below the data. DFOB = desferrioxamine B; Fh = ferrihydrite. Further details on the LC fits are shown in Figure S5.

The U EXAFS data obtained from the sediments are shown in Figure 3B. The four spectra from Steed Pond samples (sites #2300 and #2302, as whole sediments and as clay fractions) overlay each other, which indicates the same U(VI) speciation averaged over all of the U atoms in the sediment at this site, regardless of size fraction. The spectrum from #2301 was of significantly lower quality due to the lower U concentration (Table S4) and was not used. The two spectra from the Beaver Pond sediments (# 2303 and #2304) also overlay each other, indicating the same U(VI) speciation within that location. Comparisons between the averaged spectra from Steed Pond and Beaver Pond show small but consistent differences at the two sites (see arrows in Figure 3B). The corresponding differences in average U(VI) speciation are quantified in linear combination fits (see below). The Fourier transform (FT) of the data is shown in Figure 3C and consists of a main peak at R + Δ = 1.3 Å corresponding to the axial oxygens in the uranyl cation, a shoulder around R + Δ = 2.2 Å resulting from the equatorial O coordination, and a smaller peak around R + Δ = 2.8 Å corresponding to multiple-scattering (MS) contributions from the axial oxygens potentially overlaid by contributions from complexing atoms such as Fe or P atoms at the surface of a mineral or from a phosphate ligand [30,31,58,59]. No peaks are observed at larger distances in the FT, indicating that U(VI) in the sediment did not precipitate as a U(VI) mineral [60].

Shell-by-shell analysis of the data was not done, as its interpretation would be ambiguous due to the high likelihood of U(VI) in these sediments being distributed between several species, which would cause peak overlap from the shells of the different species (i.e., the measured spectrum may result from a fraction of the U being adsorbed to minerals and a fraction associated with organic matter). Instead, linear combination (LC) analysis was used to estimate the proportions of U in the different compartments. We tested the experimental data against reference spectra collected during the previous study at the same beamline, using all combinations of up to three of the following standards: aqueous U(VI) and U(VI) complexed to carboxyl ligands [33], U(VI) complexed to the siderophore desferrioxamine B (DFOB) and associated with NAu-2 clay minerals [33], a U(VI)-phosphate precipitate [61], U(VI) adsorbed on Fe or Al oxides [30], and U(VI) adsorbed on Syn-1 or NAu-2 clay minerals [30,33]. These standards were deemed representative of possible inner- and outer-sphere associations of U(VI) with organic ligands, phosphoryl/phosphate groups, or clay or oxide minerals in the sediment. The LC analysis showed that only two components were needed to reproduce the data. The best fits are shown in Figure 3D (details in Figure S5). At both field locations, U(VI) is predominantly associated with clay minerals (~65%). The remaining ~35% of the U(VI) atoms are associated with metal oxides at Steed Pond and OM ligands at Beaver Pond, corresponding to the small spectral differences observed between the two sites (Figure 3B). The partial association of U(VI) with organic ligands at Beaver Pond correlates both with the higher TOC content determined for Beaver Pond sediments (99.0 ± 23.7 g/kg of TOC) relative to Steed Pond sediments (46.7 ± 20.2 g/kg of TOC) (*t*-test, $p < 0.05$, Table 1) and with the higher proportion of the organic fraction U(VI) determined by sequential extractions (Table S5). The partial association of U(VI) with oxide surfaces at Steeds Pond determined by EXAFS does not appear to correlate with higher free Fe in the sediment (Table S2) or with higher amorphous Fe oxide-associated U in the extractions (Table S5), so this binding mode may be due to a specific Fe oxide phase/coating that is present at Steeds Pond but not present at Beaver Pond, and that is not captured by the chemical or XRD analyses. The predominant binding of U(VI) to the clay mineral surface observed by EXAFS at both sites is likely due to the high content and large reactive areas of clay minerals in the sediment, which may also be preferentially binding OM, supported by positive clay-OM correlation (Table 2 and Figure S1), and contributing to the bulk correlation observed between U and OM, as well as the predominance of organic U observed in sequential extraction (Figure 2). Such observations also corresponded well with the adsorption of U on clay minerals and OM-coated clay minerals reported in other environments [62,63]. The sequential extraction and spectroscopy yielded different relative proportions of U associated with the various solid phases. This discrepancy may, in part, be attributed to the operational definitions

of both methods. As mentioned earlier, the sequential extractions do not isolate specific processes (e.g., exchangeable) or phases (e.g., organic or iron oxide phases), but instead they generally target these specific fractions. Similarly, XAS analyses used reference materials that approximated those expected in the sample. For example, in these measurements, we defined the U-OM fraction as having similar XAS spectra as those generated by U bound to the siderophore, DFOB, and U bound to carboxyl ligands. While these are workable simplifications of natural OM, they very likely do not capture all the possible OM reactive ligands involved in U bonding. XAS is much more narrowly defined and, as such, more useful for understanding geochemical processes in such complex sediment systems.

4. Conclusions

Seven sediment samples were collected along the Tims Branch to investigate the key processes responsible for the strong U and Ni immobilization in the wetland environment. Several key findings were obtained from a series of analyses: (1) a strong correlation between sediment Ni and U concentrations was observed, suggesting that initial depositional processes may have had a greater impact on Ni and U distribution in the wetland than subsequent biogeochemical processes; (2) relatively large $K_{d-desorb}$ values for U (~4000 L/kg on average) were found in this study, suggesting that the U in Tims Branch watersheds will largely remain attached to the sediments. Much weaker binding of Ni (i.e., lower $K_{d-desorb}$) than U to these sediments indicated that Ni poses a greater long-term risk than U for migrating downstream in the dissolved form; (3) weak correlations of $K_{d-desorb}$ with different sediment characteristics were found, including pH, OM, and other sediment properties. Nevertheless, we observed a strong pH-OM coupling effect and their correlation with total U and organic fractions of U and Ni, that is, increased OM preservation resulting from the naturally acidic environment at Tims Branch (pH = 4.84 $\pm$ 0.68) promoted Ni- and especially U-sediment retention; and (4) U EXAFS data from several sediments also indicated that 65% of the U(VI) was adsorbed to mineral clay surfaces while the remainder was associated with either OM in Beaver Pond, where OM concentrations were relatively high, or to Fe-oxides in Steed Pond.

Together, these results suggest that the Tims Branch wetlands will continue to attenuate the migration of U and Ni, thereby providing a natural barrier to their transport throughout a watershed. Our study also demonstrated a delicate balance of geochemical properties that controls whether wetlands behave as sinks or sources of contaminants (e.g., the observed pH-OM coupling effect on U and Ni distributions). However, significant anthropogenic or climatic changes may disrupt the complex hydrological and biogeochemical balance necessary to maintain this long-term immobilization of metal contaminants in wetland systems. Extreme storm and flooding events may periodically lead to increased transport of contaminants-immobilized particles downstream of Tims Branch, which would require time-series monitoring and mass balance studies in future studies, especially considering the increasing extreme weather events due to climate change.

Supplementary Materials: The following supporting information can be downloaded at: https://www.mdpi.com/article/10.3390/w16070966/s1, Figure S1: Observed correlation between different sediment properties in Tims Branch sediments. Red star denotes the #2306 sample collected from the upstream of Tims Branch. Figure S2: Observed correlation of sediment properties (pH, organic matter (OM), total nitrogen) with total U/Ni concentrations or U/Ni associated with organic fraction in Tims Branch sediments. Red star denotes the #2306 sample collected from the upstream of Tims Branch. Figure S3: Desorption coefficient values of U and Ni ($K_{d-desorb}$) in the Tims Branch sediments. Figure S4: Linear combination analysis of the U XANES data from the sediments using a U(IV) standard (nanoparticulate uraninite) and a U(VI) standard (U(VI) complexed with DFOB and adsorbed to NAu-1 clay; [35]). The refined proportion of each standard spectrum is shown as % of total U in the solids. Uncertainty is estimated at $\pm$5%. Figure S5: Best fits in the linear combination (LC) analysis of the U EXAFS data from the two sediment areas. The scaled fit components are plotted below the data and fit, the vertical lines indicate the fit range, and the table lists the refined scaling factors. Uncertainty is estimated at $\pm$5%. The goodness-of-fit parameters are those calculated by

the program ATHENA [37] that was used to perform the LC fits. Table S1: Sequential Extraction Procedure. Table S2: Sediment characterization, including pH, organic matter abundance (OM), total organic carbon (TOC), total nitrogen (TN), total free Fe concentrations and the clay/silt/sand distribution. Table S3: Mineral composition of the clay-size fraction from contaminated (#2300–#2305) and upstream (#2306) sediments. Table S4: Total Ni and U concentrations and their accumulation in contaminated Tims Branch sediments, as well as the desorption coefficient values of U and Ni ($K_{d-desorb}$) and enrichment of Ni and U in clay fraction of sediments. Table S5: Concentrations and solid phase distribution (in %) of different U and Ni fractions. References [64–69] are cited in the Supplementary Materials.

Author Contributions: Conceptualization, D.I.K.; Methodology, M.I.B., E.J.O., J.S. and D.I.K.; Investigation, P.L., M.I.B., W.X., S.P.S. and D.I.K.; Data curation, P.L., M.I.B., E.J.O., S.P.S. and D.I.K.; Writing—original draft, P.L.; Writing—review & editing, P.L., M.I.B., E.J.O., K.M.K., S.P.S. and D.I.K.; Supervision, D.I.K.; Project administration, D.I.K.; Funding acquisition, D.I.K. All authors have read and agreed to the published version of the manuscript.

Funding: Support for this research came from the Wetland Hydrobiogeochemistry Scientific Focus Area (SFA) at ANL, funded by the Environmental Systems Science Program, Office of Science, Department of Energy (DOE), under contract DE-AC02-06CH11357. Other DOE funding included a Cooperative Agreement (DE-EM0005228) with SREL/UGA and funding from the minority Serving Institutions Partnership Program (TOA#0000655879). This research used resources from the Advanced Photon Source, a DOE Office of Science User Facility that is operated by ANL (contract DE-AC02-06CH11357). We thank the MRCAT/EnviroCAT beamline staff for their assistance at the synchrotron. MRCAT/EnviroCAT operations are supported by DOE and the MRCAT/EnviroCAT member institutions.

Data Availability Statement: The original contributions presented in the study are included in the article/Supplementary Materials, further inquiries can be directed to the corresponding author.

Conflicts of Interest: The authors declare no conflict of interest.

References

1. Kaplan, D.I.; Zhang, S.; Roberts, K.A.; Schwehr, K.; Xu, C.; Creeley, D.; Ho, Y.-F.; Li, H.-P.; Yeager, C.M.; Santschi, P.H. Radioiodine concentrated in a wetland. *J. Environ. Radioact.* **2014**, *131*, 57–61. [CrossRef]
2. Ramachandra, T.V.; Sudarshan, P.B.; Mahesh, M.K.; Vinay, S. Spatial patterns of heavy metal accumulation in sediments and macrophytes of Bellandur wetland, Bangalore. *J. Environ. Manag.* **2018**, *206*, 1204–1210. [CrossRef] [PubMed]
3. Li, C.; Wang, H.; Liao, X.; Xiao, R.; Liu, K.; Bai, J.; Li, B.; He, Q. Heavy metal pollution in coastal wetlands: A systematic review of studies globally over the past three decades. *J. Hazard. Mat.* **2022**, *424*, 127312. [CrossRef] [PubMed]
4. Schoner, A.; Noubactep, C.; Buchel, G.; Sauter, M. Geochemistry of natural wetlands in former uranium milling sites (eastern Germany) and implications for uranium retention. *Geochemistry* **2009**, *69*, 91–107. [CrossRef]
5. O'Geen, A.T.; Budd, R.; Gan, J.; Maynard, J.J.; Parikh, S.J.; Dahlgren, R.A. Mitigating nonpoint source pollution in agriculture with constructed and restored wetlands. *Adv. Agron.* **2010**, *108*, 1–76. [CrossRef]
6. Frohne, T.; Rinklebe, J.; Diaz-Bone, R.A. Contamination of floodplain soils along the Wupper River, Germany, with As, Co, Cu, Ni, Sb, and Zn and the impact of pre-definite redox variations on the mobility of these elements. *Soil Sediment Contam.* **2014**, *23*, 779–799. [CrossRef]
7. Llorens, E.; Matamoros, V.; Domingo, V.; Bayona, J.M.; García, J. Water quality improvement in a full-scale tertiary constructed wetland: Effects on conventional and specific organic contaminants. *Sci. Total Environ.* **2009**, *407*, 2517–2524. [CrossRef]
8. Khan, S.; Ahmad, I.; Shah, M.T.; Rehman, S.; Khaliq, A. Use of constructed wetland for the removal of heavy metals from industrial wastewater. *J. Environ. Manag.* **2009**, *90*, 3451–3457. [CrossRef]
9. Groza, N.; Manescu, A.; Panturu, E.; Filcenco-Olteanu, A.; Panturu, R.I.; Jinescu, C. Uranium wastewater treatment using wetland system. *Rev. Chim.* **2010**, *61*, 680–684.
10. Boyer, A.; Ning, P.; Killey, D.; Klukas, M.; Rowan, D.; Simpson, A.J.; Passeport, E. Strontium adsorption and desorption in wetlands: Role of organic matter functional groups and environmental implications. *Water Res.* **2018**, *133*, 27–36. [CrossRef]
11. Kaplan, D.I.; Smith, R.J.; Parker, C.J.; Roberts, K.A.; Hazenberg, P.; Morales, J.; O'Loughlin, E.J.; Boyanov, M.I.; Weisenhorn, P.; Kemner, K.M.; et al. Natuural attenuation of uranium in a fluvial weltand: Importance of hydrology and speciation. *Appl. Geol.* **2023**, *155*, 105718.
12. Mitsch, W.J.; Gosselink, J.G. *Wetlands*; John Wiley & Sons, Inc.: Hoboken, New Jersey, NJ, USA, 2015; p. 736.
13. Bertsch, P.M.; Hunter, D.B.; Sutton, S.R.; Bajt, S.; Rivers, M.L. In situ chemical speciation of uranium in soils and sediments by micro X-ray absorption spectroscopy. *Environ. Sci. Technol.* **1994**, *28*, 980–984. [CrossRef] [PubMed]

14. Evans, A.G.; Bauer, L.R.; Haselow, J.S.; Hayes, D.W.; Martin, H.L.; McDowell, W.L.; Pickett, J.B. *Uranium in the Savannah River Site Environment (No. WSRC-RP-92-315)*; Westinghouse Savannah River Co.: Aiken, SC, USA, 1992.
15. Pickett, J.B. *Heavy Metal Contamination in Tims Branch Sediments (No. OPS-RMT-900200)*; Westinghouse Savannah River Co.: Aiken, SC, USA, 1990.
16. Sowder, A.G.; Bertsch, P.M.; Morris, P.J. Partitioning and availability of uranium and nickel in contaminated riparian sediments. *J. Environ. Qual.* **2003**, *32*, 885–898. [CrossRef] [PubMed]
17. Li, D.; Seaman, J.C.; Chang, H.S.; Jaffe, P.R.; van Groos, P.K.; Jiang, D.T.; Chen, N.; Lin, J.; Arthur, Z.; Pan, Y.; et al. Retention and chemical speciation of uranium in an oxidized wetland sediment from the Savannah River Site. *J. Environ. Radio.* **2014**, *131*, 40–46. [CrossRef] [PubMed]
18. Chang, H.S.; Buettner, S.W.; Seaman, J.C.; Jaffeé, P.R.; Koster van Groos, P.G.; Li, D.; Peacock, A.D.; Scheckel, K.G.; Kaplan, D.I. Uranium immobilization in an iron-rich rhizosphere of a native wetland plant from the Savannah River Site under reducing conditions. *Environ. Sci. Technol.* **2014**, *48*, 9270–9278. [CrossRef] [PubMed]
19. Kaplan, D.I.; Kukkadapu, R.; Seaman, J.C.; Arey, B.W.; Dohnalkova, A.C.; Buettner, S.; Li, D.; Varga, T.; Scheckel, K.G.; Jaffé, P.R. Iron mineralogy and uranium-binding environment in the rhizosphere of a wetland soil. *Sci. Total Environ.* **2016**, *569*, 53–64. [CrossRef] [PubMed]
20. Kaplan, D.I.; Boyanov, M.I.; Losey, N.A.; Lin, P.; Xu, C.; O'Loughlin, E.J.; santschi, P.H.; Xing, W.; Kuhne, W.W.; Kemner, K.M. Uranium biogeochemistry in the rhizosphere of a riparian wetland. *Environ. Sci. Technol* **2024**, *in press*.
21. Punshon, T.; Gaines, K.F.; Jenkins, R.A., Jr. A. Bioavailability and trophic transfer of sediment-bound Ni and U in a southeastern wetland system. *Arch. Environ. Contam. Toxicol.* **2003**, *44*, 30–35. [CrossRef]
22. Punshon, T.; Gaines, K.F.; Bertsch, P.M.; Burger, J. Bioavailability of uranium and nickel to vegetation in a contaminated riparian ecosystem. *Environ. Toxicol. Chem. Int. J.* **2003**, *22*, 1146–1154. [CrossRef]
23. Kaplan, D.I.; Parker, C.; Powell, B.A. *Uranium Immobility in Tims Branch Wetland. No. SRNL-STI-2021-00081*; Savannah River Site (SRS): Aiken, SC, USA.; Savannah River National Lab. (SRNL), Clemson University:: Clemson, SC, USA, 2021.
24. Whittig, L.D.; Allardice, W.R. X-ray diffraction techniques. In *Methods of Soil Analysis: Part 1 Physical and Mineralogical Methods*; American Society of Agronomy, Inc.: Madison, WI, USA, 1986; Volume 5, pp. 331–362.
25. Sparks, D.L.; Page, A.L.; Helmke, P.A.; Loeppert, R.H. *Methods of Soil Analysis, Part 3: Chemical Methods*; John Wiley & Sons: Hoboken, NJ, USA, 2020.
26. EPA (Ed.) Method 3050B. Acid Digestion of Sediments, Sludges, and Soils. Revision 2. In *Test Methods for Evaluating Solid Wastes: Physical/Chemical Methods*; Environmental Protection Agency: Washington, DC, USA, 1996.
27. Ulery, A.L.; Drees, R. *Methods of Soil Analysis: Part 5-Mineralogical Methods*; Wiley Online Library: Hoboken, NJ, USA, 2008.
28. Kaplan, D.I.; Serkiz, S. Quantification of thorium and uranium sorption to contaminated sediments. *J. Radioanal. Nuclear Chem.* **2001**, *248*, 529–535. [CrossRef]
29. Segre, C.U.; Leyarovska, N.E.; Chapman, L.D.; Lavender, W.M.; Plag, P.W.; King, A.S.; Kropf, A.J.; Bunker, B.A.; Kemner, K.M.; Dutta, P.; et al. The MRCAT insertion device beamline at the Advanced Photon Source. In Proceedings of the Synchrotron Radiation Instrumentation: Eleventh U.S. National Conference, Stanford, CA, USA, 13–15 October 1999; Pianetta, P., Ed.; American Institute of Physics: New York, NY, USA, 2000; pp. 419–422.
30. Boyanov, M.I.; Latta, D.E.; Scherer, M.M.; O'Loughlin, E.J.; Kemner, K.M. Surface area effects on the reduction of U(VI) in the presence of synthetic montmorillonite. *Chem. Geol.* **2017**, *464*, 110–117. [CrossRef]
31. Boyanov, M.I.; O'Loughlin, E.J.; Roden, E.E.; Fein, J.B.; Kemner, K.M. Adsorption of Fe (II) and U (VI) to carboxyl-functionalized microspheres: The influence of speciation on uranyl reduction studied by titration and XAFS. *Geochim. Cosmochim. Acta* **2007**, *71*, 1898–1912. [CrossRef]
32. Zhang, L.; Chen, Y.; Xia, Q.; Kemner, K.M.; Shen, Y.; O'Loughlin, E.J.; Pan, Z.; Wang, Q.; Huang, Y.; Dong, H.; et al. Combined effects of Fe (III)-bearing clay minerals and organic ligands on U (VI) bioreduction and U (IV) speciation. *Environ. Sci. Technol.* **2021**, *55*, 5929–5938. [CrossRef] [PubMed]
33. Zhang, L.; Dong, H.; Li, R.; Liu, D.; Bian, L.; Chen, Y.; Pan, Z.; Boyanov, M.I.; Kemner, K.M.; Wen, J. Effect of Siderophore DFOB on U (VI) Adsorption to Clay Mineral and Its Subsequent Reduction by an Iron-Reducing Bacterium. *Environ. Sci. Technol.* **2022**, *56*, 12702–12712. [CrossRef] [PubMed]
34. Newville, M.; Livins, P.; Yacoby, Y.; Rehr, J.J.; Stern, E.A. Near-edge x-ray absorption fine structure of Pb—A comparison of theory and experiment. *Phys. Rev. B* **1993**, *47*, 14126–14131. [CrossRef] [PubMed]
35. Ravel, B.; Newville, M. Athena, Artemis, Hephaestus: Data analysis for X-ray absorption spectroscopy using IFEFFIT. *J. Synchrotron Rad.* **2005**, *12*, 537–541. [CrossRef] [PubMed]
36. Kaplan, D.I.; Xu, C.; Huang, S.; Lin, Y.; Tolic, N.; Roscioli-Johnson, K.M.; Santschi, P.H.; Jaffe, P.R. Unique organic matter and microbial properties in the rhizosphere of a wetland soil. *Environ. Sci. Technol.* **2016**, *50*, 4169–4177. [CrossRef]
37. Kaplan, D.I. *Subsurface Mobile Colloids: Their Surface Characterization, Mineralogy, and Role in Contaminant Transport in a Coastal Plain Aquifer*; Georgia University: Athens, GA, USA, 1993.
38. Wiseman, C.L.S.; Püttmann, W. Interactions between mineral phases in the preservation of soil organic matter. *Geoderma* **2006**, *134*, 109–118. [CrossRef]
39. Sarkar, B.; Singh, M.; Mandal, S.; Churchman, G.J.; Bolan, N.S. Clay minerals—Organic matter interactions in relation to carbon stabilization in soils. In *The Future of Soil Carbon*; Academic Press: Cambridge, MA, USA, 2018; pp. 71–86.

40. Kleber, M.; Bourg, I.C.; Coward, E.K.; Hansel, C.M.; Myneni, S.C.; Nunan, N. Dynamic interactions at the mineral–organic matter interface. *Nat. Rev. Earth Environ.* **2021**, *2*, 402–421. [CrossRef]
41. Stupp, S.I.; Palmer, L.C. Supramolecular Chemistry and Self-Assembly in Organic Materials Design. *Chem. Mater.* **2014**, *26*, 507–518. [CrossRef]
42. Whittinghill, K.A.; Hobbie, S.E. Effects of pH and calcium on soil organic matter dynamics in Alaskan tundra. *Biogeochemistry* **2012**, *111*, 569–581. [CrossRef]
43. Li, Q.; Wang, L.; Fu, Y.; Lin, D.; Hou, M.; Li, X.; Hu, D.; Wang, Z. Transformation of soil organic matter subjected to environmental disturbance and preservation of organic matter bound to soil minerals: A review. *J. Soils Sediments* **2023**, *23*, 1485–1500. [CrossRef]
44. Dixon, K.L. *Background Concentrations of Metals in Wetland Soils on and Near the Savannah River Site (No. WSRC-MS-97-00692-Rev. 1)*; Savannah River Site (SRS): Aiken, SC, USA, 1997.
45. Dong, W.; Tokunaga, T.K.; Davis, J.A.; Wan, J. Uranium (VI) adsorption and surface complexation modeling onto background sediments from the F-Area Savannah River Site. *Environ. Sci. Technol.* **2012**, *46*, 1565–1571. [CrossRef]
46. Virtanen, S.; Vaaramaa, K.; Lehto, J. Fractionation of U, Th, Ra and Pb from boreal forest soils by sequential extractions. *Appl. Geochem.* **2013**, *38*, 1–9. [CrossRef]
47. Skipperud, L.; Salbu, B. Sequential extraction as a tool for mobility studies of radionuclides and metals in soils and sediments. *Radiochim. Acta* **2015**, *103*, 187–197. [CrossRef]
48. Harasim, P.; Filipek, T. Nickel in the environment. *J. Elem.* **2015**, *20*, 525–534. [CrossRef]
49. Ashayeri, N.Y.; Keshavarzi, B. Geochemical characteristics, partitioning, quantitative source apportionment, and ecological and health risk of heavy metals in sediments and water: A case study in Shadegan Wetland, Iran. *Mar. Poll. Bull.* **2019**, *149*, 110495. [CrossRef]
50. Fakhradini, S.S.; Moore, F.; Keshavarzi, B.; Naidu, R.; Wijayawardena, A.; Soltani, N.; Rostami, S. Spatial distribution, partitioning, ecological risk and source apportionment of potential toxic elements in water and sediments of the Hoor Al-Azim wetland and their bioaccumulation in selected commercial fish species. *Mar. Poll. Bull.* **2021**, *172*, 112875. [CrossRef]
51. Lusa, M.; Bomberg, M. Microbial Community Composition Correlates with Metal Sorption in an Ombrotrophic Boreal Bog: Implications for Radionuclide Retention. *Soil Syst.* **2021**, *5*, 19. [CrossRef]
52. Skipperud, L.; Strømman, G.; Yunusov, M.; Stegnar, P.; Uralbekov, B.; Tilloboev, H.; Zjazjev, G.; Heier, L.S.; Rosseland, B.O.; Salbu, B. Environmental impact assessment of radionuclide and metal contamination at the former U sites Taboshar and Digmai, Tajikistan. *J. Environ. Radioact.* **2013**, *123*, 50–62. [CrossRef]
53. Manoj, S.; Thirumurugan, M.; Elango, L. Determination of distribution coefficient of uranium from physical and chemical properties of soil. *Chemosphere* **2020**, *244*, 125411. [CrossRef] [PubMed]
54. Whicker, J.J.; Pinder III, J.E.; Ibrahim, S.A.; Stone, J.M.; Breshears, D.D.; Baker, K.N. Uranium partition coefficients (Kd) in forest surface soil reveal long equilibrium times and vary by site and soil size fraction. *Health Phys.* **2007**, *93*, 36–46. [CrossRef]
55. Semião, A.J.; Rossiter, H.M.; Schäfer, A.I. Impact of organic matter and speciation on the behaviour of uranium in submerged ultrafiltration. *J. Membr. Sci.* **2010**, *348*, 174–180. [CrossRef]
56. Liu, Z.; Ou, T.; Su, M.; Peng, H.; Song, G.; Kong, L.; Chen, D. U (VI) sequestration by Al-rich minerals: Mechanism on phase dependence and the influence of natural organic matter. *Chem. Eng. J.* **2021**, *415*, 128858. [CrossRef]
57. Velasco, C.A.; Brearley, A.J.; Gonzalez-Estrella, J.; Ali, A.M.S.; Meza, M.I.; Cabaniss, S.E.; Thomson, B.M.; Forbes, T.Z.; Lezama Pachec, J.S.; Cerrato, J.M. From adsorption to precipitation of U (VI): What is the role of pH and natural organic matter? *Environ. Sci. Technol.* **2021**, *55*, 16246–16256. [CrossRef] [PubMed]
58. Dublet, G.; Pacheco, J.L.; Bargar, J.R.; Fendorf, S.; Kumar, N.; Lowry, G.V.; Brown Jr, G.E. Partitioning of uranyl between ferrihydrite and humic substances at acidic and circum-neutral pH. *Geochim. Cosmochim. Acta* **2017**, *215*, 122–140. [CrossRef]
59. Krot, A.; Vlasova, I.; Trigub, A.; Averin, A.; Yapaskurt, V.; Kalmykov, S. From EXAFS of reference compounds to U (VI) speciation in contaminated environments. *J. Synchrotron Radiat.* **2022**, *29*, 303–314. [CrossRef] [PubMed]
60. Catalano, J.G.; Brown, G.E. Analysis of uranyl-bearing phases by EXAFS spectroscopy: Interferences, multiple scattering, accuracy of structural parameters, and spectral differences. *Am. Mineral.* **2004**, *89*, 1004–1021. [CrossRef]
61. Rui, X.; Kwon, M.J.; O'Loughlin, E.J.; Dunham-Cheatham, S.; Fein, J.B.; Bunker, B.; Kemner, K.M.; Boyanov, M.I. Bioreduction of hydrogen uranyl phosphate: Mechanisms and U (IV) products. *Environ. Sci. Technol.* **2013**, *47*, 5668–5678. [CrossRef]
62. Bone, S.E.; Cliff, J.; Weaver, K.; Takacs, C.J.; Roycroft, S.; Fendorf, S.; Bargar, J.R. Complexation by organic matter controls uranium mobility in anoxic sediments. *Environ. Sci. Technol.* **2019**, *54*, 1493–1502. [CrossRef]
63. Bone, S.E.; Dynes, J.J.; Cliff, J.; Bargar, J.R. Uranium (IV) adsorption by natural organic matter in anoxic sediments. *Proc. Natl. Acad. Sci. USA* **2017**, *114*, 711–716. [CrossRef]
64. Boyanov, M.I.; Fletcher, K.E.; Kwon, M.J.; Rui, X.; O'Loughlin, E.J.; Loöffler, F.E.; Kemner, K.M. Solution and microbial controls on the formation of reduced U (IV) species. *Environ. Sci. Technol.* **2011**, *45*, 8336–8344. [CrossRef]
65. Lee, J.H.; Fredrickson, J.K.; Kukkadapu, R.K.; Boyanov, M.I.; Kemner, K.M.; Lin, X.; Kennedy, D.W.; Bjornstad, B.N.; Konopka, A.E.; Moore, D.A.; et al. Microbial reductive transformation of phyllosilicate Fe(III) and U(VI) in fluvial subsurface sediments. *Environ. Sci. Technol.* **2012**, *46*, 3721–3730. [CrossRef]
66. *D 5074-90*; Standard Practice for Preparation of Natural-Matrix Sediment Reference Samples for Major and Trace Inorganic Constituents Analysis by Partial Extraction Procedures. The Annual Book of ASTM Standards. American Society for Testing and Materials: Philadelphia, PA, USA, 1990.

67. *D 3974-81*; Standard Practices for Extraction of Trace Elements from Sediments. The Annual Book of ASTM Standards. American Society for Testing and Materials: Philadelphia, PA, USA, 1990.
68. Miller, W.P.; Martens, D.C.; Zelazny, L.W.; Kornegay, E.T. Forms of solid phase copper in copper-enriched swine manure. *J. Environ. Qual.* **1986**, *15*, 69–72. [CrossRef]
69. Rhoades, J.D. Salinity: Electrical Conductivity and Total Dissolved Solids. In *Methods of Soil Analysis, Part 3, Chemical Methods*; Sparks, D.L., Ed.; Soil Science Society of America Press: Madison, WI, USA, 1996; pp. 417–436.